Nanostructures

DOI: 10.1002/anie.200803231

Emergent Hybrid Nanostructures Based on Non-Equilibrium Block Copolymer Self-Assembly**

*Mei Li and Stephen Mann**

Functional materials based on the self-assembly of amphiphilic block copolymers have attracted considerable interest in areas such as pharmaceutics and separation systems,[1–4] artificial vesicles,[5,6] templating of inorganic mesostructures,[7,8] and fabrication of linear or spatially separated arrays of metallic nanoparticles.[9,10] Amphiphilic block copolymers display diverse lyotropic phase behaviour such that a variety of supramolecular structures in the form of spherical or cylindrical micelles, hexagonal, cubic or bicontinuous liquid crystals, and unilamellar or multilamellar spherical vesicles can be assembled spontaneously depending on polymer molecular weight and concentration, block length and composition, solvent composition and temperature.[11,12] Whilst such structures provide important functional platforms for the design of hybrid nanostructures incorporating drug sequestration, biomolecule encapsulation or inorganic templating, their shape and dynamical properties are generally restricted by equilibrium considerations. As a consequence, there are few reports for example on the spontaneous self-assembly of block copolymers into highly elongated tubular nanostructures; indeed, such architectures are generally produced by sequential processing involving for example the step-wise chemical degradation or hydrolysis of the core domains of cylindrical micelles rather than by de novo self-organization.[13–16] It seems feasible that increases in both functionality and structural complexity could be achieved in block copolymer nanostructures by adopting non-equilibrium self-assembling systems, particular those exhibiting emergent behaviour. There are precedents for this approach in the use of conventional surfactants in reactive microemulsion systems that are subjected to temporally and spatially dependent mesoscale transformations involving metastable surfactant–inorganic hybrid nanostructures.[17] Moreover, similar mechanisms may account for the unusual neuron-like calcium phosphate/polymer nanostructures produced in the presence of a poly(ethylene oxide)-*b*-polymethacrylic acid ($E_{68}MA_6$) block copolymer in which the MA domain was partially alkylated with dodecylamine.[18]

In general, however, there are few studies on the spontaneous assembly of amphiphilic block copolymers into kinetically trapped and dynamically active states because compared with conventional surfactants the increased molecular weight and hence decreased mobility of amphiphilic block copolymers restrict transformation of these systems into non-equilibrium metastable states. It is notable, therefore, that Ryan et al. have recently reported the formation of myelin-like multilamellar tubular structures when the diblock copolymer amphiphile, poly(ethylene oxide)-*b*-poly(1,2-butylene oxide) ($E_{16}B_{22}$), was placed in contact with water.[19] Myelin structures are complex multilamellar tubes produced by diffusional growth associated with the interfacial transition of a swollen lamellar phase to multilamellar vesicles in the presence of excess solvent. The solvent gradient induces surface wrinkling and unbinding of the lamellar phase, which result in hemispherical outgrowths that develop into highly elongated multilamellar extensions by inward diffusion of solvent at the roots of the swollen tubes.[20] As a consequence, the myelin outgrowths represent metastable intermediates between the gel-like lamellar phase and dispersed multilamellar vesicles, and although in local equilibrium with the surrounding solvent, they are kinetically trapped and therefore readily destabilised by changes in the concentration gradient and exposure to shear forces and electric fields.

Silica–polymer myelin nanostructures were produced by addition of aqueous NH_4OH to mixtures of tetraethyl orthosilicate (TEOS) and $E_{16}B_{22}$ at respective molar ratios between 0.6:1 and 10:1 (see Supporting Information). Sonication of the reaction mixtures, which contained a polymer concentration of 1 wt% in water, resulted in turbid aqueous suspensions of gel-like polymer–TEOS particles that gradually transformed into myelin structures within a period of 3–5 days at 22–25 °C. SEM images showed an extensive network of intact myelin filaments that were soft, flexible and unbranched, and many tens of micrometres in length (Figure 1). Similar images were observed by atomic force microscopy (Supporting Information, Figure S1). The filaments were highly uniform in width, capped at their ends, and smooth-sided or surface-roughened depending on the TEOS:$E_{16}B_{22}$ molar ratio used. Significantly, control experiments undertaken in the absence of TEOS indicated that myelin structures were not obtained under the above conditions; instead, myelins formed from the swollen lamellar $E_{16}B_{22}$ particles were observed to rapidly transform into multilamellar vesicles. Thus, the formation of myelin nanostructures could be significantly stabilized by incorporating TEOS into the polymer phase prior to dispersion and swelling in alkaline aqueous solutions. Indeed, the silica–polymer nanostructures remained structurally intact within the reaction solution for at least two months.

Studies of samples extracted from the reaction mixture during the early stages of formation indicated that the

[*] Dr. M. Li, Prof. S. Mann
Centre for Organized Matter Chemistry, School of Chemistry, University of Bristol, Bristol BS8 1TS (UK)
E-mail: s.mann@bristol.ac.uk

[**] We thank EPSRC (Platform grant EP/C518748/1) for financial support.

Supporting information for this article is available on the WWW under http://dx.doi.org/10.1002/anie.200803231.

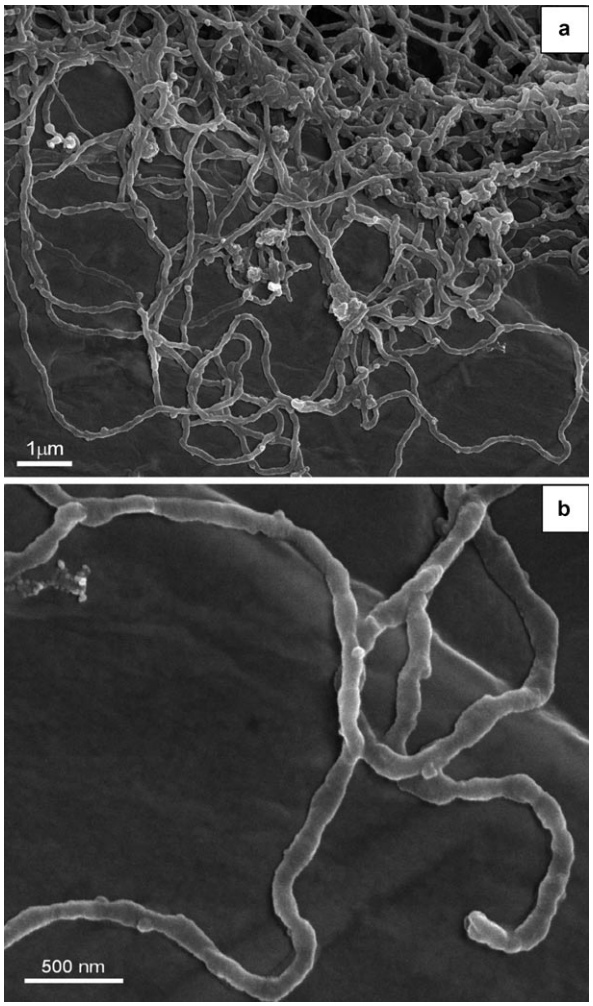

Figure 1. SEM images of silica–polymer myelin nanocomposites at a) low and b) high magnification.

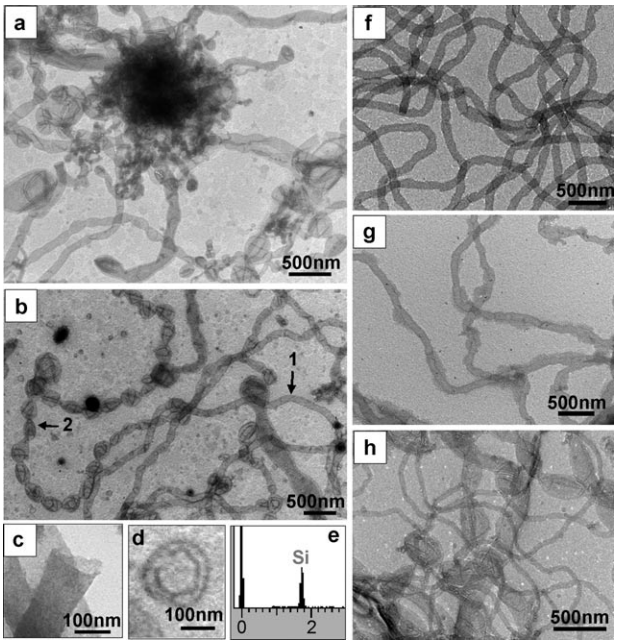

Figure 2. a) TEM image of initial growth stage showing silica–myelin outgrowths from a primary $E_{16}B_{22}$–TEOS particle. b–e) TEM data for silica–polymer myelin nanostructures produced at a TEOS:$E_{16}B_{22}$ molar ratio of 0.6:1, and [$E_{16}B_{22}$] = 1 wt% in water; b) smooth-sided (arrow 1) and twisted nanostructures with bulbous instabilities (arrow 2); c) broken silica–polymer nanostructure confirming tubular morphology; d) cross-sectional view showing silicification of inner and outer walls of a multilamellar myelin tube; e) EDX analysis of a single nanotube showing the Si peak. f,g) TEM images of silica–polymer myelins prepared at TEOS:$E_{16}B_{22}$ molar ratios of 3.6:1 (f) and 7.4:1 (g) showing highly uniform or roughened nanotubes, respectively. h) TEM image of silica–myelin sample after heating the TEM grid to 400 °C to produce intact replicas in the form of well-defined silica nanofilaments.

filaments originated as finger-like outgrowths from the primary polymer–TEOS particles, confirming the classical myelin-induced mechanism of structure evolution (Figure 2a). At a relatively low silica content (TEOS:$E_{16}B_{22}$ = 0.6:1), TEM images showed a range of structures, predominantly smooth-sided filaments (Figure 2b, arrow 1) that were shown to be tubular in morphology (Figure 2c) with an average width of 116 nm ($\sigma = 22$) (Supporting Information, Figure S2). The electron density associated with filaments viewed in cross-section indicated that the ultrathin silica sheath was 10–20 nm in thickness, and deposited specifically on the inner and outer surface of a multilamellar polymer tube (Figure 2d). In addition, twisted nanotubes, budded filaments, as well as tubes comprising chains of bulbous swellings (pearl instabilities)[19] that were approximately 200–250 nm across were observed (Figure 2b, arrow 2). Such structures represent intermediate forms associated with the transformation of myelins into vesicles in the presence of relatively high water contents. In each case, EDX analysis on the different myelin forms showed a Si peak at 1.7 keV (Figure 2e), indicating that the tubular forms were silica–$E_{16}B_{22}$ hybrid nanocomposites. Electron diffraction analysis of individual nanostructures, as well as XRD studies of whole samples (data not shown), showed only a very broad peak centred at $2\theta = 22°$, indicating that the polymer–inorganic hybrids were amorphous. Increasing the concentration of TEOS, for example to a TEOS:$E_{16}B_{22}$ molar ratio of 1.8:1, produced a similar range of silica–polymer myelins, whereas higher silica levels (TEOS:$E_{16}B_{22}$ = 3.6:1) gave rise to highly uniform smooth-sided tubules with increased electron density associated with the elevated silica content (Figure 2f). No pearl instabilities, twisted cylinders or vesicles were observed, indicating that under these conditions, silica mineralization was highly effective in stabilizing the polymer myelin structures and inhibiting the onset of transformation to vesicular forms. Further increases in silica content (TEOS:$E_{16}B_{22}$ = 7.4:1 or 10:1) resulted in myelin filaments with partially roughened surfaces due to excess silica mineralization on the external surface of the polymer filaments (Figure 2g).

The formation of integrated silica–polymer myelin nanocomposites was confirmed by FTIR spectroscopy (Supporting Information, Figure S3a). The FTIR spectrum of the hybrid materials showed typically strong vibration peaks for $E_{16}B_{22}$,

for example at 1105 cm^{-1} (C–O–C) and 2875–2964 cm^{-1} (CH_2, CH_3). Significantly, the intensity ratio of these two peaks (I_{1105}/I_{2876}), which was almost 1:1 in the pure polymer, increased progressively as the silica content was raised, (Supporting Information, Figure S3b), consistent with the superimposition of polymer (C–O–C) and silica (Si–O–Si) absorption bands in this region of the spectrum. Changes in the intensity ratio showed a distinct plateau region for TEOS:$E_{16}B_{22}$ molar ratios between 3 and 6, followed by a secondary increase in the values of I_{1105}/I_{2876}. The results indicated that surface coverage of the polymer nanostructures was established at a TEOS:polymer molar ratio of ca. 4:1, and that this overlayer could then be further thickened by additional silica mineralization. This was consistent with the TEM observations shown in Figure 2g.

Removal of the polymer template from the myelin nanocomposites to produce intact silica replicas was achieved by heating samples dried onto TEM grids up to a temperature of 400 °C for 2 h. FTIR spectra showed a broad Si–O–Si peak at 1100 cm^{-1} along with negligible absorbance in the CH_2/CH_3 region around 2875–2964 cm^{-1} (Supporting Information, Figure S3a), confirming that the polymer had been burnt out under these conditions. The corresponding TEM images of the thermally treated sample showed continuous silica nanotubules with smooth edges or bulbous pearl instabilities that appeared to be high definition facsimiles of the hybrid precursor nanostructures (Figure 2h).

The above results indicate that diblock polymer myelin nanotubes can be stabilized in aqueous solutions with respect to transformation into spherical vesicles by in situ hydrolysis and condensation of TEOS molecules organized within dispersed particles of a swollen lamellar phase of $E_{16}B_{22}$. Static 1D ^1H NMR spectra indicated that there was minimal chemical interaction between the polymer and TEOS in the absence of water or aqueous NH_4OH. Specifically, a viscous liquid of $E_{16}B_{22}$ showed broad resonances corresponding to the propyl side chain (singlet $\delta_{CH_3} = 0.98$ ppm; doublet $\delta_{CH_2} = 1.52/1.60$ ppm) and polymer backbone ($\delta = 3.35$ to 3.62 ppm), which shifted downfield by only 0.08 ppm on addition of TEOS to the liquid polymer at a TEOS:$E_{16}B_{22}$ mole ratio of 4:1. In addition, an upfield shift was observed in the resonances of the added TEOS (from $\delta = 1.54$ to 1.33 and 4.13 to 3.92 ppm for δ_{CH_3} and δ_{CH_2}, respectively), which were attributed solely to solvent effects. Corresponding SAXS profiles of the liquid $E_{16}B_{22}$ copolymer showed a single broad peak centred at a spacing of 5.5 nm, which remained effectively unchanged for a 4:1 $E_{16}B_{22}$/TEOS mixture (Figure 3a,b). This bilayer spacing was double that determined previously for dried samples of $E_{16}B_{22}$,[13] suggesting that the polymer chains were partially hydrated. Significantly, addition of aqueous NH_4OH (pH 10.8) or water (pH 7) to the polymer–TEOS mixture gave a relatively sharp single peak in the SAXS profile (Figure 3c), which corresponded to a markedly increased interlamellar spacing of 15.8 nm associated with the gel-like polymer particles. In contrast, addition of aqueous NH_4OH to $E_{16}B_{22}$ in the absence of TEOS produced a swollen lamellar phase but with a spacing (11.3 nm) that was significantly less than that observed in the presence of both NH_4OH and TEOS (Figure 3d).

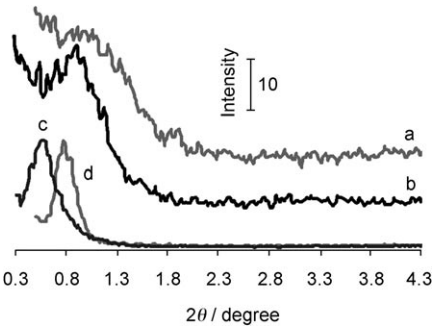

Figure 3. SAXS profiles for a) $E_{16}B_{22}$, b) $E_{16}B_{22}$/TEOS, c) $E_{16}B_{22}$/TEOS + aqueous NH_4OH, and d) $E_{16}B_{22}$ + aqueous NH_4OH. The profiles have been offset vertically to aid presentation.

As the SAXS experiments were recorded within 2–3 h of addition of the aqueous phase, and in contrast myelin outgrowth occurred over a period of 3–5 days, the above results reflected structural changes occurring specifically within the precursor gel-like particles. Addition of TEOS to liquid $E_{16}B_{22}$ did not have a significant effect on the lamellar mesostructure of the polymer, but addition of water to the polymer in the absence of TEOS produced a doubling of the interlayer spacing. Significantly, incorporation of TEOS into the lamellar polymer phase and treatment with aqueous NH_4OH or water produced an additional 4.5 nm expansion of the hydrated mesostructure. We attribute this change to intercalation between the polymer bilayers of a mixture of hydrolysed inorganic species (silicic acid, silicate oligomers, etc.) rather than an extended condensed phase of hydrated amorphous silica. This was consistent with the use of aqueous NH_4OH as a base catalyst at pH 10.8, which is known to promote hydrolysis but not condensation,[14] and was supported by analogous experiments undertaken in aqueous HCl that did not produce well-defined myelin nanocomposites due to an increased level in the rate of silica condensation (data not shown). Indeed, the observed ability of the highly swollen intercalated nanocomposite to undergo transformation into myelin suggests that the nanocomposite precursor is sufficiently soft and fluid to adapt dynamically to progressive ingress of solvent without loss of the mesolamellar structure. Moreover, the high fidelity of spontaneous co-organization observed in the anisotropic hybrid nanostructures suggests that myelin growth and formation of extended silicified structures are coupled by outward diffusion of both $E_{16}B_{22}$ molecules and silicate precursors into regions of high solvent concentration. As a consequence, emergence of the multilamellar myelin filaments is concurrent with silica deposition on the inner and outer surfaces of the polymer tubes to produce hybrid constructs that are structurally stabilized with respect to further transformation into vesicles. In this regard, kinetic trapping of the myelin form is critically dependent on the silica:polymer mole ratio, which strongly influences the rates of diffusion and condensation of the hydrolysed silicate species at the myelin–solvent interface.

We extended the above experiments to produce silica–$E_{16}B_{22}$ myelin nanostructures with a range of additional

functionalities (Supporting Information, Figure S4). Addition of tetraethyl orthotitanate (TEOTi) to the above reaction system at a TEOS:$E_{16}B_{22}$:TEOTi molar ratio of 3.6:1:0.11 resulted in the formation of highly extended polymer–inorganic myelin structures comprising both amorphous silica and titania. Alternatively, thiol-functionalized organosilica–$E_{16}B_{22}$ myelin nanotubes could be readily prepared from aqueous dispersions of gel-like polymer particles comprising mixtures of TEOS and up to 50 mol% of 3-mercaptopropyl triethoxysilane (MPTES). Addition of a citrate-stabilized Au sol to a dispersion of the thiol-functionalized silica–myelin nanotubes produced composite filaments that were highly decorated with metallic nanoparticles. Corresponding UV/Vis spectra showed a shift in the surface plasmon band from 520 nm to 650 nm, consistent with surface-induced aggregation of the metallic particles on the organosilica–$E_{16}B_{22}$ myelin nanotubes. In contrast, no binding of the Au nanoparticles was observed in the presence of silica–polymer myelin nanostructures prepared from TEOS alone, confirming the high affinity of the pendent mercaptopropyl groups for nanoparticle adsorption along the external surface of the hybrid nanotubes.

As silica, as well as poly(ethylene oxide)-based polymers,[21] are well recognized as biocompatible materials, silica–$E_{16}B_{22}$ myelins should have potential applications in diverse areas involving drug and biomolecule delivery. As proof-of-principle, we tested the ability of the silica–$E_{16}B_{22}$ nanotubes to adsorb and release the anti-inflammatory drug ibuprofen, which has medium water solubility. Silica–polymer myelins were prepared as above but in the presence of aqueous NH_4OH containing 10 mM of the drug. FTIR spectra of dried samples after removal of excess ibuprofen showed a carbonyl vibration peak at 1723 cm^{-1}, indicating the presence of ibuprofen in the hybrid materials. Time-dependent profiles of drug release from the hybrid nanostructures showed a slow but steady increase in the solution concentration of ibuprofen over a period of 24 h (Figure 4 and Supporting Information, Figure S5), indicating that the hydrated silica walls were sufficiently porous to permit ibuprofen diffusion. In contrast, drug release from non-silicifed $E_{16}B_{22}$ was much faster particularly in the first 5 h after immersion in water, indicating that the silica phase was effective at attenuating the initial release kinetics.

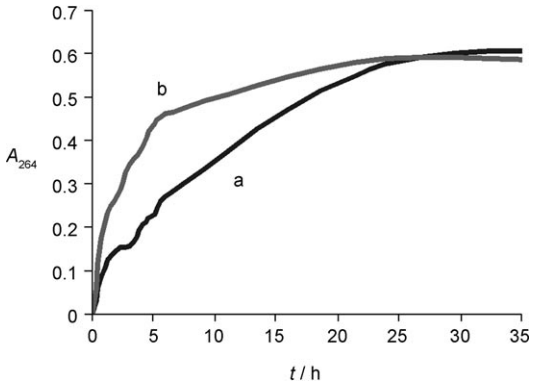

Figure 4. Plot of absorbance at 264 nm with time for a) ibuprofen-containing silica–$E_{16}B_{22}$ nanotubes and b) ibuprofen–myelin control sample without silica.

The above results illustrate the potential for controlling the functionalization of polymer–inorganic nanotubes prepared by emergent assembly of myelin nanostructures. Clearly, the stabilization conferred on the polymer myelins through integration of silica at the nanoscale level could be a key factor in enabling future materials developments and potential applications. For example, the extremely high shape anisotropy, confined interior micro-environment, and propensity for in situ growth extension and alignment could be exploited to create interfacial structures and networks that adapt and respond in time and space to stimuli in the local environment. Indeed, the use of emergent nanostructures opens up the possibility of producing components that have primitive life-like properties.[22]

Received: July 3, 2008
Revised: August 27, 2008
Published online: October 23, 2008

Keywords: block copolymers · hybrid nanostructures · non-equilibrium structures · self-assembly

[1] M. L. Adams, A. Lavasanifar, G. S. Kwon, *J. Pharm. Sci.* **2003**, *92*, 1343.
[2] S. E. Dunn, A. Brindley, S. S. Davis, M. C. Davies, L. Illum, *Pharm. Res.* **1994**, *11*, 1016.
[3] Y. Kim, P. Dalhaimer, D. V. Christian, D. E. Discher, *Nanotechnology* **2005**, *16*, S484.
[4] C. Allen, J. Han, K. Yu, D. Maysinger, A. Eisenberg, *J. Controlled Release* **2000**, *63*, 275.
[5] D. E. Discher, A. Eisenberg, *Science* **2002**, *297*, 967.
[6] W. Meier, C. Nardin, M. Winterhalter, *Angew. Chem.* **2000**, *112*, 4747; *Angew. Chem. Int. Ed.* **2000**, *39*, 4599.
[7] B. Smarsly, S. Polarz, M. Antonietti, *J. Phys. Chem. B* **2001**, *105*, 10473.
[8] C. G. Göltner, B. Smarsly, B. Berton, M. Antonietti, *Chem. Mater.* **2001**, *13*, 1617.
[9] X. S. Wang, H. Wang, N. Coombs, M. A. Winnik, I. Manners, *J. Am. Chem. Soc.* **2005**, *127*, 8924.
[10] H. Wang, W. Lin, WK. P. Fritz, G. D. Scholes, M. A. Winnik, I. Manners, *J. Am. Chem. Soc.* **2007**, *129*, 12924.
[11] P. Bhargava, Y. Tu, J. X. Zheng, H. Xiong, R. P. Quirk, S. Z. D. Cheng, *J. Am. Chem. Soc.* **2007**, *129*, 1113.
[12] S. Jain, F. S. Bates, *Science* **2003**, *300*, 460.
[13] K. Yu, A. Eisenberg, *Macromolecules* **1998**, *31*, 3509.
[14] X. Yan, G. Liu, F. Liu, B. Z. Tang, H. Peng, A. B. Pakhomov, C. Y. Wong, *Angew. Chem.* **2001**, *113*, 3705; *Angew. Chem. Int. Ed.* **2001**, *40*, 3593.
[15] J. Raez, I. Manners, M. A. Winnik, *J. Am. Chem. Soc.* **2002**, *124*, 10381.
[16] M. Reches, E. Gazit, *Science* **2003**, *300*, 625.
[17] H. Cölfen, S. Mann, *Angew. Chem.* **2003**, *115*, 2452; *Angew. Chem. Int. Ed.* **2003**, *42*, 2350.
[18] L. Qi, H. Cölfen, M. Antonietti, M. Li, J. D. Hopwood, A. J. Ashley, S. Mann, *Chem. Eur. J.* **2001**, *7*, 3526.
[19] G. Battaglia, A. J. Ryan, *Angew. Chem.* **2006**, *118*, 2106; *Angew. Chem. Int. Ed.* **2006**, *45*, 2052.
[20] M. Buchanan, S. U. Egelhaaf, M. E. Cates, *Langmuir* **2000**, *16*, 3718.
[21] J. Hyung Park, Y. H. Bae, *J. Biomed. Mater. Res.* **2003**, *64*, 309.
[22] S. Mann, *Angew. Chem.* **2008**, *120*, 5386; *Angew. Chem. Int. Ed.* **2008**, *47*, 5306.

